Princeton Plasma Physics Laboratory

PPPL- 4960

PPPL- 4960

Theory Verification and Numerical Bnchmarking on Neoclassical Toroidal Viscosity Torque

Z. Wang, et. al.

DECEMBER, 2013

Prepared for the U.S. Department of Energy under Contract DE-AC02-09CH11466.

Princeton Plasma Physics Laboratory
Report Disclaimers

Full Legal Disclaimer

Trademark Disclaimer

PPPL Report Availability

Princeton Plasma Physics Laboratory:

http://www.pppl.gov/techreports.cfm

Office of Scientific and Technical Information (OSTI):

http://www.osti.gov/bridge

Related Links:

U.S. Department of Energy

Office of Scientific and Technical Information

Fusion Links

Theory verification and numerical benchmarking on neoclassical toroidal viscosity torque

December 10, 2013

Zhirui Wang*, Jong-Kyu Park*, Yueqiang Liu[1], Nikolas Logan*, Kimin Kim*, Jonathan E. Menard*

* Princeton Plasma Physics Laboratory Princeton, New Jersey 08543, USA

1 Euratom/CCFE Association, Culham Science Centre, Abingdon, OX14 3DB, United Kingdom

Abstract

Systematic verification and numerical benchmarking have been successfully carried out among three different approaches of neoclassical toroidal viscosity (NTV) theory and the corresponding codes: IPEC-PENT is developed based on the combined NTV theory but without geometric simplifications [1]; MARS-Q includes smoothly connected NTV formula [2] based on Shaing's analytic formulation in various collisionality regimes; MARS-K, originally computing the drift kinetic energy, is upgraded to compute the NTV torque based on the equivalence between drift kinetic energy and NTV torque [3]. The derivation and numerical results both indicate that the imaginary part of drift kinetic energy computed by MARS-K is equivalent to the NTV torque in IPEC-PENT. In the benchmark of precession resonance between MARS-Q and MARS-K/IPEC-PENT, the agreement and correlation between the connected NTV formula and the combined NTV theory in different collisionality regimes is shown for the first time. Additionally, both IPEC-PENT and MARS-K indicate the importance of the bounce harmonic resonance which can greatly enhance the NTV torque when $\mathbf{E} \times \mathbf{B}$ drift frequency reaches the bounce resonance condition.

1 Introduction

It is known that the toroidal asymmetry produced by non-axisymmetric magnetic perturbations in tokamaks can cause a substantial damping of toroidal flow through the neoclassical toroidal viscosity (NTV) torque. Therefore, the NTV torque can provide a promising way to externally optimize plasma rotation and rotation shear thereby improving plasma instabilities and performance, as has been highlighted by recent experiments [4–8]. In order to increase the predictability for NTV and the controllability for plasma rotation in tokamaks, it is important to understand the different approaches of NTV theory with proper cross-benchmark.

To study the NTV physics, various semi-analytic methods have been developed in recent years. In general, the methods find the NTV torque by solving the bounce averaged drift kinetic equation with approximations which depend on the approaches. There are mainly three different approaches with corresponding codes established. In the first approach, following the combined NTV theory [1] but without the geometric simplification, the IPEC-PENT code [9] is developed to perform the NTV computation with an effective Krook collisional operator, where the torque caused by the resonance with the precession motion ($l = 0$) and the particle bounce motion ($l \neq 0$) of trapped particles are considered. Here l denotes the Fourier harmonic number of bounce motion. The effects due to different particle motions are combined by a generalized equation. The second approach, extensively developed by Shaing [2], focuses on the precession motion of trapped particles. A simple connection formula is used to smoothly connect the formulations in different collisionality regimes - the so called smoothly connected NTV formula. The analytic formulation with an appropriate simplification of toroidal geometry has been derived by considering the separation of collisionality regimes. Particularly, in this approach, the full pitch angle scattering collisional operator is included, which can be more accurate and important in the low collisionality regime. This semi-analytic approach has been implemented in MARS-Q [22, 23]. The third approach is based on the equivalence between the drift kinetic energy and the NTV torque due to trapped particles as shown in Ref. [3]. Similar to the NTV torque caused by magnetic perturbations, the drift kinetic theory in the study of the ideal MHD stability of modes, such as the resistive wall mode (RWM) [10–17], takes into account the mode-particle interaction derived from the perturbed drift kinetic

equation. The MARS-K code [18], which has been applied to the RWM studies, is upgraded to compute the NTV torque following this approach. The NTV torque due to precession and bounce resonances of trapped particles are included in the code.

In the present work, a systematic verification of these three different NTV approaches, as well as a numerical benchmarking among IPEC-PENT and MARS-K/Q, is carried out. This paper is organized as follows. Section 2 describes the model of ideal perturbed equilibrium and the neoclassical toroidal viscosity models in IPEC-PENT and MARS-K/Q. The equivalence between the combined NTV torque and drift kinetic energy in MARS-K is demonstrated. Section 3 reports the benchmark results of perturbed equilibrium, as well as the NTV torques computed by IPEC-PENT, MARS-K/Q with respect to the three different approaches. The NTV torques due to the precession resonance ($l = 0$) and bounce resonance ($l \neq 0$) of trapped ions are investigated. Section 4 summarizes the work.

2 Models and formulations

2.1 Ideal Perturbed equilibrium model

The IPEC-PENT code solves the ideal perturbed equilibrium (1) based on the perturbed force balance [24] in toroidal system. The force balance equation is linearized in the presence of the external perturbed field,

$$\vec{j} \times \vec{B} + \vec{J} \times \vec{b} - \nabla p = 0, \tag{1a}$$

$$p = -\vec{\xi} \cdot \nabla P - \Gamma P \nabla \cdot \vec{\xi}, \tag{1b}$$

$$\vec{b} = \nabla \times (\vec{\xi} \times \vec{B}), \tag{1c}$$

$$\vec{j} = \nabla \times \vec{b}. \tag{1d}$$

The perturbed quantities $\vec{\xi}$, $\vec{b}$, $\vec{j}$, and p denote the plasma displacement, magnetic field, current and pressure, respectively. $\vec{B}$, $\vec{J}$, P and ρ represent the equi-

librium variables of magnetic filed, current, fluid pressure and plasma density on the unperturbed flux surface. $\Gamma = 5/3$ is the ratio of specific heats.

Since the perturbed equilibrium is a linear problem and unperturbed equilibria are axisymmetric in tokamaks, the toroidal harmonic numbers n are decoupled and can be treated separately. Therefore, only a single toroidal mode number n needs to be considered at one time. The external perturbation is assumed to have an $\exp(in\phi)$ dependence along the torodial angle ϕ in both IPEC-PENT and MARS-K/Q.

MARS-K and MARS-Q are the two versions of MARS code with different modules dedicated to the computation of drift kinetic energy and NTV torque respectively, therefore the fluid part of MARS-K/Q solves the same linearized MHD equations in the toroidal geometry,

$$(\frac{\partial}{\partial t} + in\Omega)\vec{\xi} = \vec{v} + (\vec{\xi}\cdot\nabla\Omega)R^2\nabla\phi, \tag{2a}$$

$$\rho(\frac{\partial}{\partial t}+in\Omega)\vec{v} = -\nabla p+\vec{j}\times\vec{B}+\vec{J}\times\vec{b}-\rho[2\Omega\vec{Z}\times\vec{v}+(\vec{v}\cdot\nabla\Omega)R\hat{\phi}]-\nabla\cdot(\rho\vec{\xi})\Omega\vec{Z}\times\vec{V}_0, \tag{2b}$$

$$(\frac{\partial}{\partial t} + in\Omega)\vec{b} = \nabla\times(\vec{v}\times\vec{B}) + (\vec{b}\cdot\nabla\Omega)R\hat{\phi} - \nabla\times(\eta\vec{j}), \tag{2c}$$

$$(\frac{\partial}{\partial t} + in\Omega)p = -\vec{v}\cdot\nabla P - \Gamma P\nabla\cdot\vec{v}, \tag{2d}$$

$$\vec{j} = \nabla\times\vec{b}, \tag{2e}$$

where $\vec{v}$ is the perturbed velocity of the plasma, R is the plasma major radius, $\hat{\phi}$ is the unit vector along the geometric toroidal angle ϕ of the torus, $\vec{Z}$ is the unit vector in the vertical direction in the poloidal plane. $\vec{V}_0$ is the plasma equilibrium flow $\vec{V}_0 = R\Omega\hat{\phi}$, with Ω being the angular frequency of the toroidal rotation. A conventional unit system is assumed with the vacuum permeability $\mu_0 = 1$. On the right hand side of equation (2b), the fourth and fifth terms represent the Coriolis force and the centrifugal force respectively.

For the purpose of plasma response modeling to the external perturbation in MARS-K/Q, the vacuum field equations outside the plasma, the thin resistive wall

equation (when applicable), and the coil equations [19] are solved together with the MHD equations for the plasma in MARS-K/Q.

It is noted that when $\partial/\partial t \to 0$ and ignoring the plasma flow, inertia and resistivity, MARS-K/Q can physically recover equation (1) to solve the perturbed equilibrium.

To compare the perturbed equilibrium computed by IPEC-PENT and MARS-K/Q, the external magnetic perturbation is generated by a source current $\vec{j}_{coil}$ flowing in the coil located in the vacuum region satisfying,

$$\nabla \times \vec{b} = \vec{j}_{coil},\ \nabla \cdot \vec{j}_{coil} = 0.$$

2.2 NTV models

2.2.1 Combined NTV model in IPEC-PENT

IPEC-PENT computes the NTV torque derived from the volume integral of the general relation,

$$T_\phi = \int dx^3 \left(\frac{\partial \vec{x}_L}{\partial \phi} \cdot \nabla \cdot \overleftrightarrow{\Pi} \right), \tag{3}$$

where $\vec{x}_L$ is the Lagrangian displacement, $\overleftrightarrow{\Pi} = p_\perp \overleftrightarrow{I} + (p_\parallel - p_\perp)\vec{b}\vec{b}$ is the anisotropic perturbed pressure tensor, $\vec{b} = \vec{B}/B$ is the unit vector of the equilibrium magnetic field, and B is the strength of the equilibrium field. The parallel and perpendicular components of the kinetic pressure $p_\parallel$ and $p_\perp$ are defined by

$$p_\parallel = \sum_{\alpha=e,i} \int d\Gamma M_\alpha v_\parallel^2 f_L^1, \tag{4}$$

$$p_\perp = \sum_{\alpha=e,i} \int d\Gamma \frac{1}{2} M_\alpha v_\perp^2 f_L^1. \tag{5}$$

The summation in equation (4) and (5) is over the electron and ion components. The integral is carried out over the velocity space of trapped particles, where

$$d\Gamma = \frac{2\pi}{M_\alpha^2} \sum_\sigma d\varepsilon_k d\mu \frac{B}{|v_\parallel|}. \tag{6}$$

Here M_α is the particle mass of ions or electrons, $v_\parallel$ and $v_\perp$ are the parallel and perpendicular velocity components of the particle, and σ=sign($v_\parallel$). The perturbed particle distribution function f_L^1 is derived by solving the bounce averaged perturbed drift kinetic equation [3] for each particle species. The neoclassical toroidal torque in terms of the kinetic pressure can be written as

$$T_\phi = -\int dx^3 \left[\left(p_\parallel - p_\perp\right) \frac{1}{B} \frac{\partial \delta B_L}{\partial \phi} + p_\parallel \frac{\partial}{\partial \phi} (\nabla \cdot \vec{\xi}) \right], \tag{7}$$

where $\delta B_L = Q_{L\parallel} + \nabla B \cdot \vec{\xi}_\perp$ as the Lagrangian quantity is the variation of the field strength measured on the perturbed field lines, $Q_{L\parallel} = \vec{b} \cdot \nabla \times (\vec{\xi}_\perp \times \vec{B})$ is the magnetic perturbation in parallel direction of the equilibrium magnetic field, and $\vec{\xi}_\perp$ is the plasma displacement perpendicular to the equilibrium field line. Following the derivation in [3], the neoclassical toroidal torque of IPEC-PENT in the approximation of zero banana orbit width can be further written as

$$T_\phi = -n^2 \sum_{\alpha=e,i} \frac{1}{ZeM_\alpha^2} \int d\psi_p d\phi \int d\varepsilon_k d\mu \sum_l \mathcal{R}_l \left|\delta J_l\right|^2 \frac{\partial f_0}{\partial \psi_p}, \tag{8}$$

where f_0 is the Maxwellian equilibrium distribution function of thermal particles. $\varepsilon_k = \varepsilon - Ze\Phi$, where ε is the particle's total energy, ε_k the kinetic energy of the particle, Φ the equilibrium electrostatic potential, and Ze the species charge (positive for ions and negative for electrons). The bounce-average action for the l-class of trapped particles is

$$\delta J_l = \tau_b \left\langle \left[(2\varepsilon_k - 3\mu B) \frac{\delta B_L}{B} + 2(\varepsilon_k - \mu B) \nabla \cdot \vec{\xi}_\perp \right] \mathcal{P}_l \right\rangle, \tag{9}$$

with an appropriate phase factor of trapped particles $\mathcal{P}_l = e^{-il\omega_b t}$ [3]. l is the number of bounce harmonics. The resonant operator of trapped particles is defined as

$$\mathcal{R}_l = \frac{\omega_b \nu_{Dl} \hat{\varepsilon}_k^{-3/2}}{[l\omega_b - n(\omega_E + \omega_d)]^2 + \nu_{Dl}^2 \hat{\varepsilon}_k^{-3}}, \tag{10}$$

where ω_d is the magnetic precession frequency of trapped particles (ions or electrons) averaged over the bounce orbit, and ω_b is the bounce frequency of trapped particles. $\nu_{Dl} = \nu_\alpha/(2\epsilon)[1 + (l/2)^2]$, with $\alpha = i, e$ defined in [1, 3] is the effective ion and electron collision frequency, $\nu_i = \nu_{ii}$ and $\nu_e \sim \nu_{ei}, \nu_{ee}$. ν_{ii},ν_{ei} and ν_{ee} are

ion-ion, electron-ion and electron-electron collision frequencies respectively in [27]. $\epsilon \approx r/R$, where r is the minor radius. ω_E is the $\mathbf{E}\times\mathbf{B}$ drift due to the equilibrium electrostatic potential. $\hat{\varepsilon}_k = \varepsilon_k/T$ is the particle kinetic energy normalized by the temperature T. When $l = 0$, the precession motion of trapped particles can resonate with plasma $\mathbf{E}\times\mathbf{B}$ flow, $\omega_d \sim \omega_E$, the so-called precession resonance. As for $l \neq 0$, the bounce resonance can occur when $n\omega_E$ is comparable with $l\omega_b$.

2.2.2 The equivalence between Kinetic energy in MARS-K and NTV in IPEC-PENT

MARS-K computes the drift kinetic energy δW_k through the kinetic pressure, $p_\parallel$ and $p_\perp$. In MARS-K, f_L^1 in equation (4) and (5) is derived by solving the perturbed drift kinetic equation following approaches by Porcelli [20]. Though Porcelli's approach allows MARS-K to include the finite banana orbit width effects, they are neglected here for benchmarking with IPEC-PENT. Particularly, in the derivation of f_L^1, it is important to note that the second term in equation (22) from [20] is equivalent to the third term of LHS in equation (1) from [1]. This term is responsible for the radial drift of trapped particle banana orbits in a 3D field. This radial drift of banana orbits eventually creates the equivalent radial current that generates toroidal torque in NTV theory. f_L^1 in MARS-K is written as

$$f_L^1 = -f_\varepsilon^0 \varepsilon_k e^{-i\omega t - in\phi} \sum_{m,l} X_m H_{ml} \lambda_l e^{in\tilde{\phi}(t) + im<\dot{\chi}>t + il\omega_b t}, \tag{11}$$

where f_ε^0 is the energy derivative of the thermal particle equilibrium distribution function (Maxwellian). $\tilde{\phi}(t) = \phi(t) - <\dot{\phi}>t$, where $<\cdot>$ denotes the average over the particle bounce period. m corresponds to the Fourier harmonic number along poloidal angle. X_m and H_{ml}, defined in [18], are related to the perturbed particle Lagrangian H_L

$$H_L = \frac{1}{\varepsilon_k}[Mv_\parallel^2 \vec{\kappa}\cdot\vec{\xi}_\perp + \mu(\vec{Q}_{L\parallel} + \nabla B\cdot\vec{\xi}_\perp)], \tag{12}$$

where $\vec{\kappa} = (\vec{b}\cdot\nabla)\vec{b}$ is the magnetic curvature, and $\mu = Mv_\perp^2/2B$ the particle magnetic moment.

The factor λ_l represents the mode-particle resonance operator,

$$\lambda_l = \frac{n[\omega_{*N} + (\hat{\varepsilon}_k - 3/2)\omega_{*T} + \omega_E] + \omega}{n\omega_d - l\omega_b + n\omega_E + \omega + i\nu_{Dl}\hat{\varepsilon}_k^{-3/2}}, \tag{13}$$

where ω_{*N} and ω_{*T} are the diamagnetic drift frequencies associated with the plasma density and temperature gradients, respectively.

With the anisotropic kinetic pressure tensor, the drift kinetic energy of trapped particles is obtained,

$$\delta W_k = \frac{1}{2}\int dx^3 \left[p_\perp \frac{1}{B}(\vec{Q}_{L\|} + \nabla B \cdot \vec{\xi}_\perp) + p_\| \vec{\kappa} \cdot \vec{\xi}_\perp \right]. \tag{14}$$

Substituting equations (4),(5), and (11)-(13) into (14), the drift kinetic energy contributed by the trapped particles in MARS-K can be further written as

$$\delta W_k = -\frac{\pi}{2}\sum_{\alpha=e,i}\frac{1}{M_\alpha^2}\int d\psi_p d\phi \int d\varepsilon_k d\mu \sum_l \frac{\partial f_0}{\partial \varepsilon}\lambda_l \tau_b \left| \left\langle \varepsilon_k H_L e^{-il\omega_b t} \right\rangle_l \right|^2. \tag{15}$$

Considering the perturbed equilibrium, $\omega \to 0$, one gets

$$\frac{\partial f_0}{\partial \psi_p} = Ze\left[\omega_{*N} + (\hat{\varepsilon}_k - 3/2)\,\omega_{*T} + \omega_E\right]\frac{\partial f_0}{\partial \varepsilon}. \tag{16}$$

The relation of the resonant operators between λ_l in MARS-K and $\mathcal{R}_l$ in IPEC-PENT is,

$$Im\left(\lambda_l\right)\frac{\partial f_0}{\partial \varepsilon} = -\frac{n}{Ze\omega_b}\frac{\partial f_0}{\partial \psi_p}\mathcal{R}_l. \tag{17}$$

Substituting equations (12) and (17) into (15) with $\omega = 0$, the equivalence between the imaginary part of δW_k in MARS-K and T_ϕ by combining equations (8)-(10) in IPEC-PENT can be established

$$T_\phi = -2nIm(\delta W_k), \tag{18}$$

which agrees with the conclusion in [3]. It indicates that MARS-K has the capability to perform the computation of neoclassical toroidal viscosity torque based on equation (18). Note that the NTV torque computed by IPEC-PENT can also be converted to δW_k based on Ref [3].

2.2.3 Connected NTV in MARS-Q

MARS-Q is a version of MARS that computes NTV torque based on the connected NTV formula in Hamada coordinate [22,23,26]. In this model, the precession resonance ($l = 0$) of trapped particles and a pitch angle scattering collisional operator are taken into account but no bounce resonance ($l \neq 0$) of trapped particles is included. The form of the torque density used in MARS-Q can be written as

$$T_{NTV} = -\tau_{NTV}^{-1} \left\langle R^2 \right\rangle_{\psi_p} \rho_i \omega_\phi, \tag{19}$$

$$\tau_{NTV}^{-1} = \frac{R_0^2}{\langle R^2 \rangle_{\psi_p}} \sum_{\alpha=i,e} \frac{\sqrt{\epsilon} q^2 \omega_{ti}^2}{2\sqrt{2}\pi^{3/2}} \left| \frac{Z_i}{Z_\alpha} \right| \times \lambda_1, n \left(1 - \frac{\omega_{nc,n}}{\omega_\phi} \right), \tag{20}$$

$$\lambda_{l,n} = \frac{1}{2} \int_0^\infty I_{\kappa n}(\hat{\varepsilon}_k)(\hat{\varepsilon}_k - 5/2)^{l-1} \hat{\varepsilon}_k^{5/2} e^{-\hat{\varepsilon}_k} d\hat{\varepsilon}_k, \tag{21}$$

where R_0 is the plasma major radius at plasma center, ρ_i is the ion mass density, $\omega_\phi = \vec{V} \cdot \nabla\phi$ is the ion flow in toroidal direction, $< \cdot >_{\psi_p}$ denotes the flux surface average, q is the safety factor, and Z_α is the charge number of α species. The ion transit frequency ω_{ti}, and $\omega_{nc,n}$, related to diamagnetic frequencies, are defined in [26].

The analytic solutions of $I_{\kappa n}$ in $1/\nu$, $\nu - \sqrt{\nu}$ and super-banana plateau regimes (SBP) are defined as $I_{\kappa n,1/\nu}$, $I_{\kappa n,\nu-\sqrt{\nu}}$ and $I_{\kappa n,sbp}$ respectively in [2, 26]. The following smoothly connected formula of $I_{\kappa n,}$ in these regimes is considered when MARS-Q solves the NTV torque.

$$I_{\kappa n,C}(\hat{\varepsilon}_k) = \begin{cases} \frac{I_{\kappa n,\nu-\sqrt{\nu}}}{1+I_{\kappa n,\nu-\sqrt{\nu}}/I_{\kappa n,1/\nu}} & (\hat{\varepsilon}_k < x_{min}), \\ \frac{I_{\kappa n,sp}}{1+I_{\kappa n,sp}/I_{\kappa n,1/\nu}} & (\hat{\varepsilon}_k \geq x_{min}), \end{cases} \tag{22}$$

where $x_{min} = |\omega_E/\omega_{B0}|$, ω_{B0} is the magnetic drift of the deeply trapped particles with $\hat{\varepsilon}_k = 1$.

It is known that the electron collisionality ν_e and the bounce frequency of electrons are normally larger than $\mathbf{E} \times \mathbf{B}$ drift frequency and ν_i. Therefore, the NTV torque is usually dominated by the contribution of ions, particularly in the bounce resonance case. However, when the collisionality is low, the NTV torque due to the precession resonance of trapped electrons can also be important [26]. In order to simplify the comparison and show a clear correlation among the three

approaches, the following discussion will only focus on the ion contributed NTV torque.

3 Numerical results

3.1 Perturbed Equilibrium

We consider a simple tokamak equilibrium with a circular cross-section which is stable to the ideal kink mode. The toroidal field at the magnetic axis $R_0 = 2\text{m}$ is assumed to be $B_0 = 1.0\text{T}$. The aspect ratio is $R/a = 10$, where a is the minor radius of plasma. The safety factor profile is shown in figure 1, where $q_0 = 1.1$ and $q_a = 2.52$. The ion and electron density have $n_i = n_e$, the ion density n_{i0} and electron density n_{e0} at plasma center vary from 10^{18} m^{-3} to 10^{21} m^{-3}. The plasma pressure profile $P = n_i T_i + n_e T_e$ is fixed. Therefore, the ion temperature T_i and electron temperature T_e, with $T_i = T_e$, are varied from 6.05 keV to 3×10^{-2} keV correspondingly, where only the thermal particles are considered. IPEC-PENT and MARS-K/Q use this equilibrium to compute the perturbed equilibrium and to numerically verify the equivalence between the NTV torque and the drift kinetic energy. For the sake of simplicity, a uniform profile of $\mathbf{E} \times \mathbf{B}$ drift frequency is considered in this work.

In order to compute the NTV torque and the drift kinetic energy, the equilibrium needs to be perturbed by the external field. The same external magnetic perturbations are applied in IPEC-PENT and MARS-K/Q to obtain the perturbed equilibrium. A continuous coil is located close to plasma, $b_c = 1.10a$. By assuming a coil current with a single helical component $(3, 1)$, the coil can generate radial magnetic perturbations dominated by the $(m, n) = (3, 1)$ harmonic at the plasma edge. Figure 2 shows the perturbed quantities (the normal displacement and the normal magnetic perturbation) computed by MARS-K/Q and IPEC-PENT respectively. Each poloidal harmonic of the perturbations in the plasma has a very good agreement between IPEC-PENT and MARS-K/Q. This ensures that the three codes are using the same perturbed equilibrium while computing the NTV torque. Since the generated external field is dominated by the $(3, 1)$ harmonic having a strength of 1 gauss at the plasma edge where $q_a < 3$, the (3,1) perturbation inside the plasma has the strongest response and penetrates into the plasma

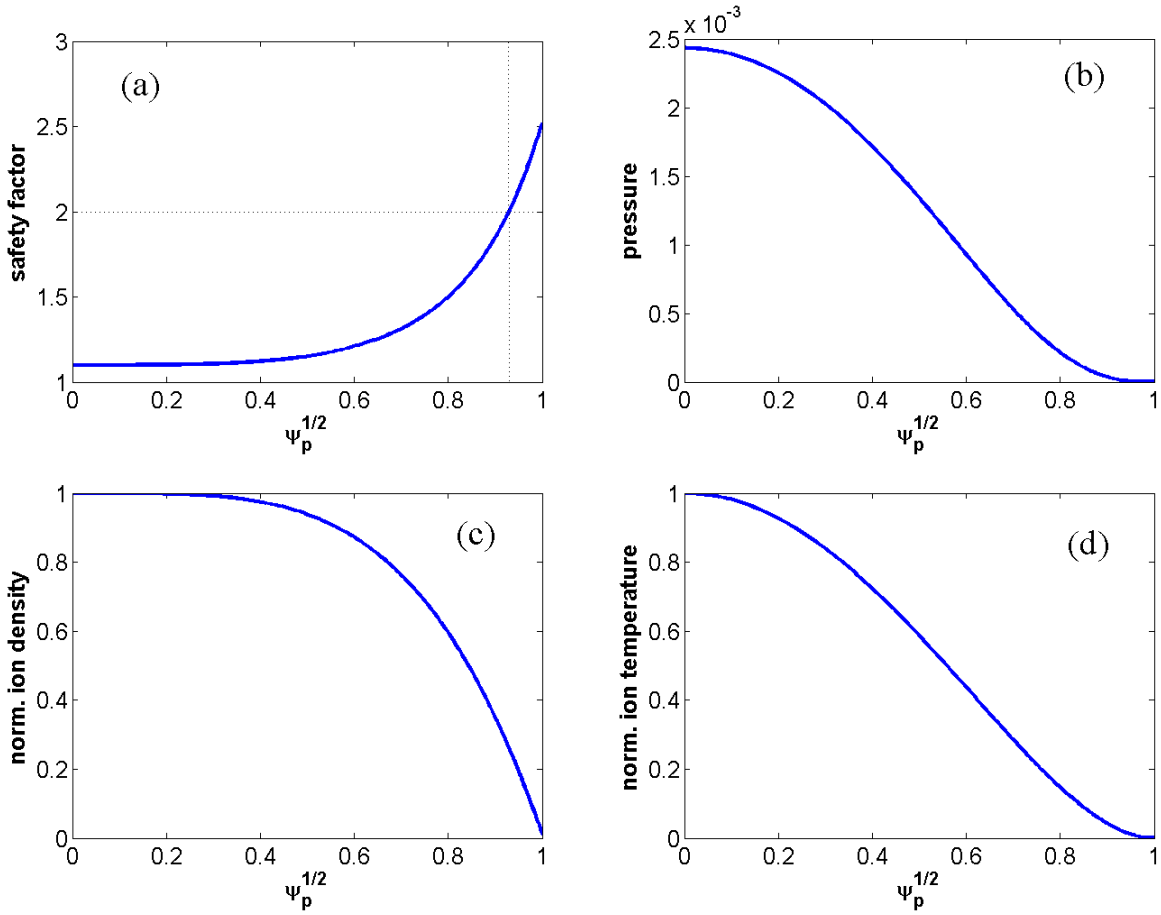

Figure 1: The safety factor q (a), the equilibrium pressure (b), ion density (c) and ion temperature (d) profiles are plotted as functions of $s = \psi_p^{1/2}$. The pressure is normalized by B_0^2/μ_0. The plasma density and the temperature profiles are normalized to unity at the magnetic axis.

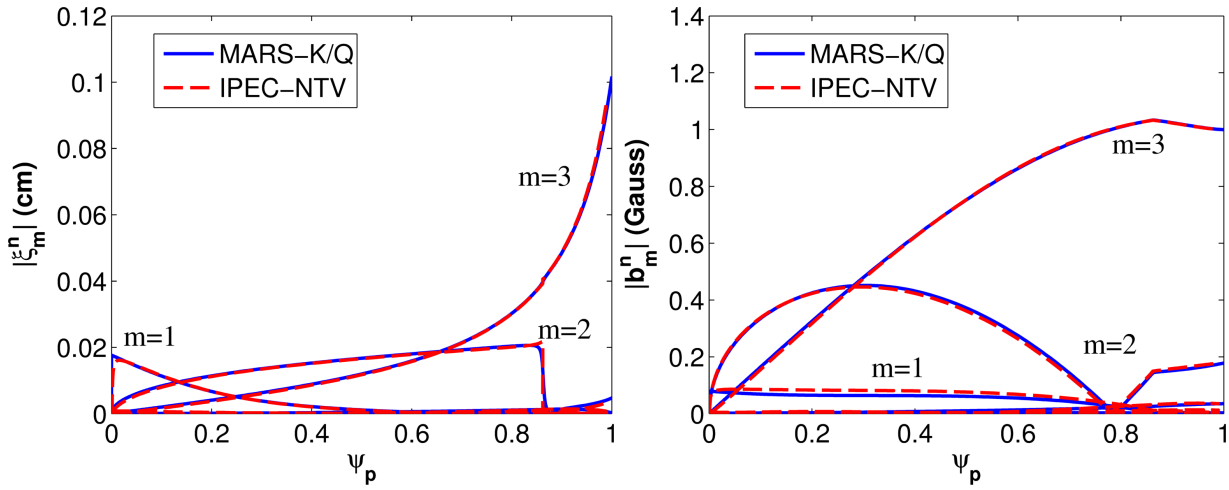

Figure 2: Comparison of radial profiles of the normal displacement (a) and the normal magnetic perturbation (b) in the presence of an external radial field dominated by $(m, n) = (3, 1)$. The poloidal harmonics of plasma response computed by MARS-K/Q (solid lines) and IPEC-PENT (dashed lines) get a excellent quantitative agreement. PEST coordinates are adopted.

without the screening effect. The toroidal coupling enhanced by the finite equilibrium pressure leads to the finite value of other harmonics, e.g $m = 1$ and $m = 2$ perturbations.

3.2 Numerical results of NTV torque

3.2.1 NTV due to precession resonance of trapped ions

In this section, we first compare the NTV torque contributed solely by the precession motion of trapped ions, based on the perturbed equilibrium described in section 3.1. In order to better understand the behavior of NTV torque in different collisionality regimes, figure 3 plots the profiles of magnetic precession frequency ω_d and bounce frequency ω_b of trapped ions which are averaged over the velocity space and the flux surface. The averaged ion magnetic precession frequency is about $10^{-3}\omega_A$. Since $\omega_d \sim 1/r$, the magnetic precession frequency increases near the plasma center. The averaged ion bounce frequency is around $5 \times 10^{-3}\omega_A$.

In figure 4, two cases, with $\omega_E = 10^{-3}\omega_A \sim < \omega_d >$, and $\omega_E = 0.1\omega_A \gg < \omega_d >$, are chosen to study the collisionality dependence of NTV torque contributed

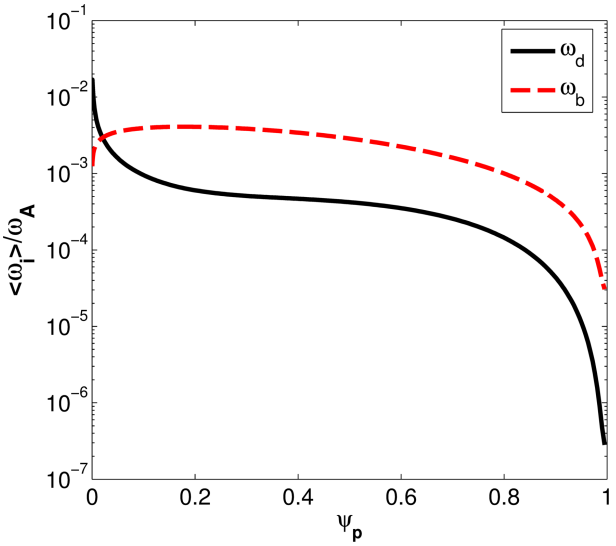

Figure 3: Radial profiles of magnetic precession frequency (ω_d) and bounce frequency (ω_b) of trapped ions averaged over the velocity space and over the flux surface. The frequencies are normalized by the Alfvén frequency ω_A at the plasma center.

by the precession resonance. The effective ion collisionality profile used in MARS-K (solid), MARS-Q(o) and IPEC-PENT(+) is varied by changing the ion density profile n_i. $\nu_i(0)$ denotes the effective ion collision frequency at the plasma center. The NTV torque T_ϕ^{MARS-K} computed by MARS-K and T_ϕ^{IPEC} by IPEC-PENT shows a very good quantitative agreement. In super-banana plateau (SBP) regime, we note that T_ϕ^{MARS-K} and T_ϕ^{IPEC} are almost independent of the collisionality which is consistent with the analytical result in [21]. As for the torque T_ϕ^{MARS-Q} computed by MARS-Q, the tendency of T_ϕ^{MARS-Q} also agrees with T_ϕ^{MARS-K} and T_ϕ^{IPEC} qualitatively. The plateau connecting the ν and $1/\nu$ regimes is found by the three codes. In fact, the two cases with low and high ω_E correspond to the resonant and non-resonant cases in [25] respectively. Since the Krook operator is used in MARS-K and IPEC-PENT, the two codes can recover the ν and $1/\nu$ regimes. The connected NTV theory includes the physics of boundary layer due to the pitch angle scattering effect. Therefore, MARS-Q can resolve the $\nu - \sqrt{\nu}$ and $1/\nu$ regimes. Figure 4 shows that T_ϕ^{MARS-Q}'s torque is larger in the $\nu - \sqrt{\nu}$ regime where MARS-Q can be more accurate than the other two codes. In the $1/\nu$

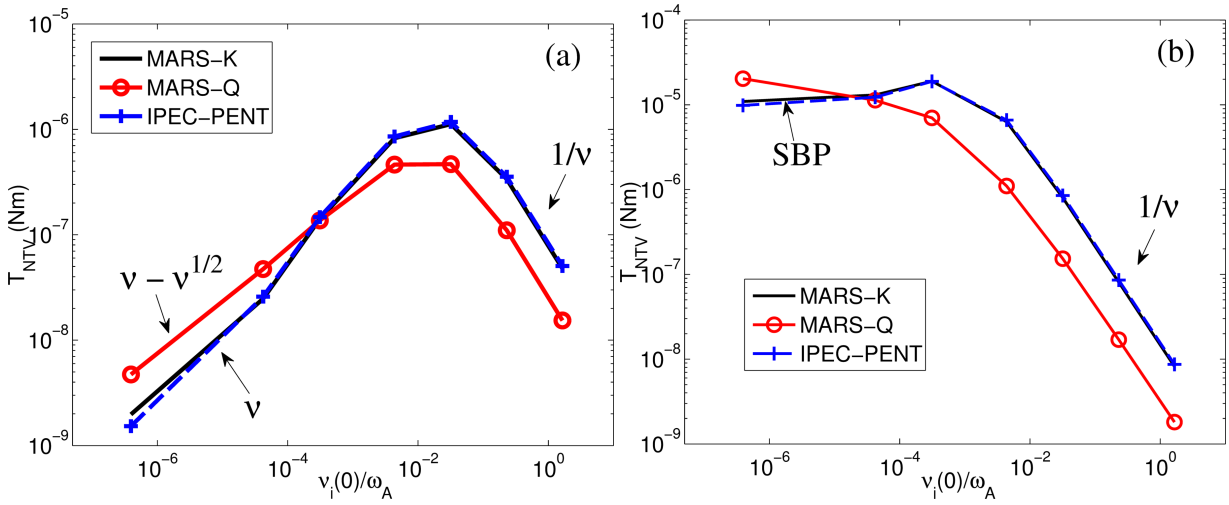

Figure 4: The comparison of the collisionality dependence of NTV torque contributed by the magnetic precession resonance of trapped ions with (a) $\omega_E = 0.1\omega_A$ and (b) $\omega_E = 10^{-3}\omega_A$. $\nu_i(0)$ is the ion effective collision frequency at plasma center.

regime, MARS-Q computes a smaller torque than T_ϕ^{MARS-K} and T_ϕ^{IPEC}. While further increasing $\nu_i(0) \to \infty$, the factor of 2 difference [25] of the torque due to the difference between the pitch angle scattering operator and Krook operator can be recovered by MARS-Q and IPEC-PENT/MARS-K.

Figure 5 shows the comparison of the torques computed by MARS-K/Q and IPEC-PENT while scanning $\mathbf{E} \times \mathbf{B}$ rotation frequency ω_E. MARS-K and IPEC-PENT again agree well. The tendency of the torque computed by MARS-Q also agrees with MARS-K and IPEC-PENT results. Figure 5(a) with low collisionality $\nu_i(0) = 4.2 \times 10^{-5}\omega_A$ shows that the torque T_ϕ decreases monotonically while the value of ω_E increases. In the high collisionality case, figure 5(b) indicates that, when $\omega_E \sim 10^{-3}\omega_A$ which is much smaller than the effective collision frequency $\nu_i(0) = 0.23\omega_A$, the variation of NTV torque T_ϕ becomes less sensitive to the change of ω_E. When $\omega_E \sim \omega_A$ is much larger than $\nu_i(0)$, similar to figure 5(a), T_ϕ monotonically decreases. These two types of behavior at $\omega_E \gg \nu_i, \omega_d$ and $\nu_i \gg \omega_E, \omega_d$ can be understood by the following simple analysis. In the rotation scan of ω_E, the torque is approximately proportional to the resonant operator $Im(\lambda_l)$ with $\omega = 0$. When $\omega_E \gg \nu_i, \omega_d$, it has $T_\phi \sim \nu_i \hat{\varepsilon}^{-3/2}/\omega_E$ which is monotonically decreased while increasing the value of ω_E. For the case $\nu_i \gg \omega_E, \omega_d$, $T_\phi \sim$

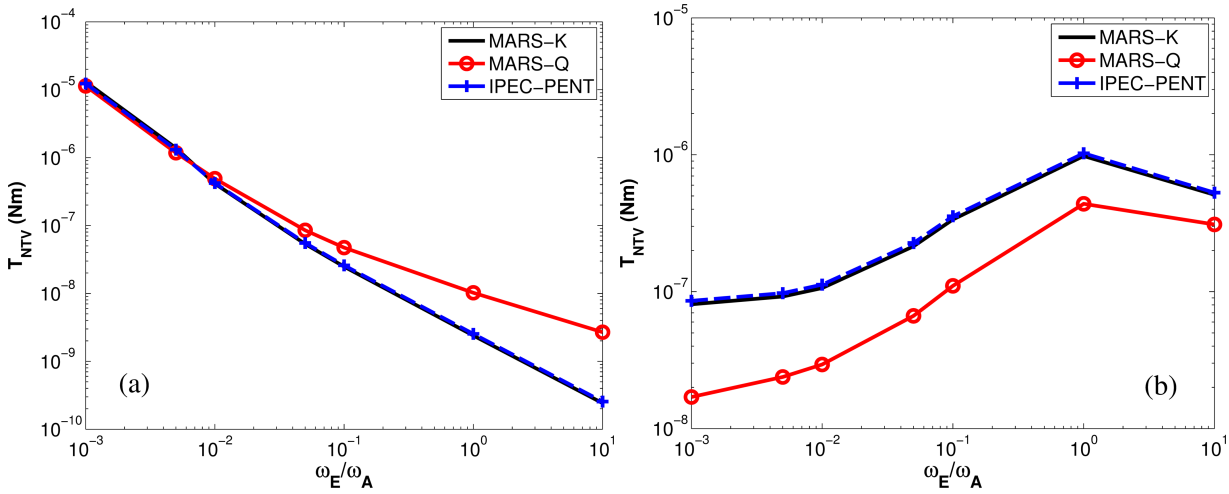

Figure 5: NTV torque due to the magnetic precession motion of trapped ions is plotted as the function of ω_E. The comparison of torque among MARS-K (solid), MARS-Q ('o') and IPEC-PENT ('+') is made with (a) $\nu_i(0) = 4.2 \times 10^{-5}$ and (b) $\nu_i(0) = 0.23$.

$[\omega_{*N} + (\hat{\varepsilon}_k - 3/2)\omega_{*T}]\,\hat{\varepsilon}_k^{3/2}/\nu_i$ indicates the torque is independent of $\mathbf{E} \times \mathbf{B}$ drift frequency.

Figure 6 compares the torque density profiles computed by MARS-K, MARS-Q and IPEC-PENT with $\omega_E = 10^{-3}$ and $\nu_i(0) = 4.2 \times 10^{-5}$. It shows that the torque profile computed by MARS-K is very close to IPEC-PENT's result. MARS-Q, which takes into account the different collisionality model and certain geometric simplifications, also presents a similar torque density profile. The above benchmarking results present a good validation of all three codes for the NTV computations contributed by the precession resonance of trapped particles.

3.2.2 NTV due to bounce motion of trapped ions

Since both the combined NTV theory and the drift kinetic energy can further include the effect of bounce motion of trapped particles (so called bounce resonance ($l \neq 0$) in NTV calculation), these effects in IPEC-PENT and MARS-K are compared in this section. To better understand the effect of bounce resonance, the conventional regimes of collisionality in terms of precession resonance are still used in the following discussion. Figure 7 compares the computed torque by IPEC-

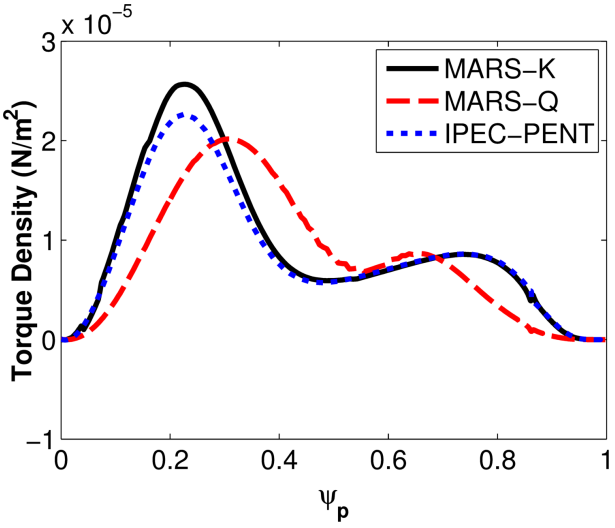

Figure 6: The torque density profiles computed by MARS-K (solid), MARS-Q (dashed) and IPEC-PENT (dotted) are compared, where $\omega_E = 10^{-3}\omega_A$ and $\nu_i(0) = 4.2 \times 10^{-5}\omega_A$. Only the precession resonance of trapped ions is considered.

PENT and MARS-K while varying the collisionality ν_i. It shows that the NTV torque computed by the two codes agree very well while including both precession and bounce resonances (total l case). Moreover, comparing with the precession resonance, it is noted that the bounce resonance can enhance the torque in the ν regime and also slightly increase the torque in the SBP regime. But the torque in the $1/\nu$ regime is dominated by the precession resonance.

The rotation scan of torque with low collisionality $\nu_i(0) = 4.2\times10^{-5}\omega_A$ in figure 8 clearly shows that the bounce resonance starts to play a major role when the ω_E rotation is comparable with the averaged ion bounce frequency $< \omega_b > \sim 5 \times 10^{-3}\omega_A$. However, when $\omega_E \gg < \omega_b >$, the contribution due to bounce resonance becomes smaller. The torque is mainly contributed by the precession resonance, when $\mathbf{E} \times \mathbf{B}$ drift frequency is far from the bounce frequency.

In the presence of precession and bounce resonances, figure 9 also shows a quantitative agreement of torque profiles computed by IPEC-NTV and MARS-K. The different numerical treatment in the two codes causes the slight discrepancy of torque profile near plasma edge but does not affect the agreement between T_ϕ^{MARS-K} and T_ϕ^{IPEC}. In this case with $\omega_E = 10^{-2}\omega_A$ and $\nu_i(0) = 4.2 \times 10^{-5}\omega_A$, the bounce resonance has a significant contribution to NTV toque. The torque

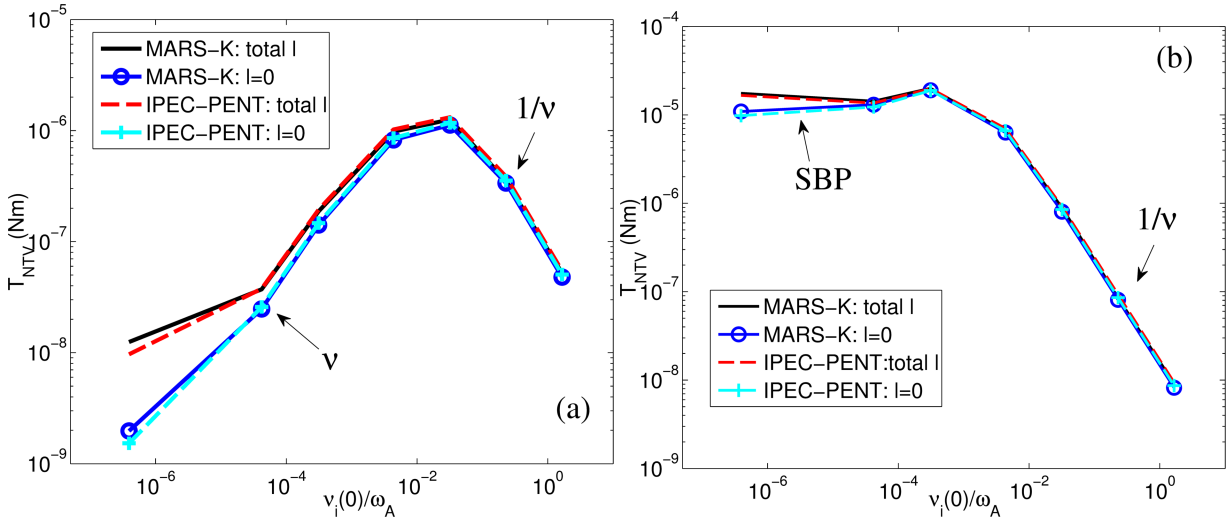

Figure 7: The collisionality dependence of NTV torque with (a) $\omega_E = 0.1\omega_A$ and (b) $\omega_E = 10^{-3}\omega_A$. MARS-K (solid and 'o') and IPEC-PENT (dashed and '+') computes two cases respectively: 1) total l case, both precession resonance ($l = 0$) and bounce resonance ($l \neq 0$) are included; 2) $l = 0$ case, only the precession resonance is considered.

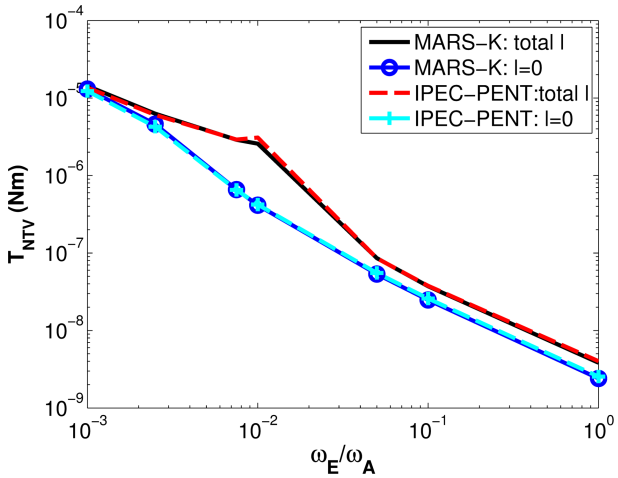

Figure 8: NTV torque is plotted as the function of ω_E with $\nu_i(0) = 4.2 \times 10^{-5}$. MARS-K (solid and 'o') and IPEC-PENT (dashed and '+') computes two cases respectively: 1) total l case, both precession resonance ($l = 0$) and bounce resonance ($l \neq 0$) are included; 2) $l = 0$ case, only the precession resonance is considered.

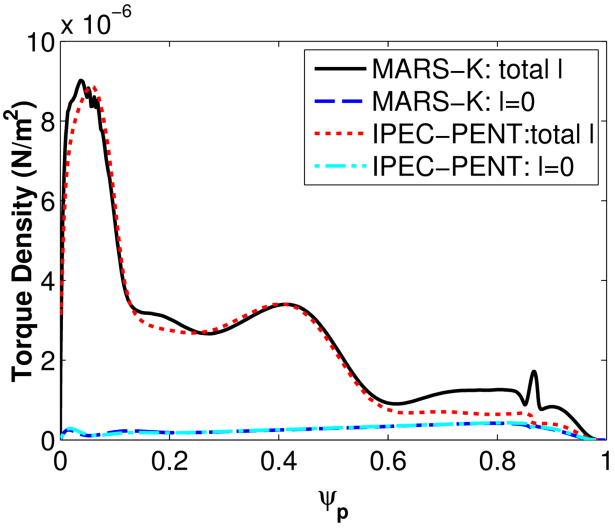

Figure 9: The torque density profiles computed by MARS-K (solid and dashed) and IPEC-PENT (dotted and dotted dash) are compared for the total l case and l=0 case denoted in figure 7, where $\omega_E = 10^{-2}\omega_A$ and $\nu_i(0) = 4.2 \times 10^{-5}\omega_A$.

profile shows that the contribution of bounce resonance is dominant everywhere along the radial direction.

Finally, to clarify in which regime the precession resonance and the bounce resonance can be important, we perform 2D scans of the NTV torque in terms of ω_E and ν_i. Figure 10(a) presents the distribution of torque only including precession resonance. A large torque due to precession resonance mainly occurs in the SBP regime, the ν regime with low ω_E and $1/\nu$ regime with low ν_i. Figure 10(a) shows that the precession resonance contributes a large plateau between ν and $1/\nu$ regimes.

Figure 10(b), only considering the bounce resonance, shows that the bounce resonance can induce a strong torque in similar regimes as the precession resonance except the plateau regime. Particularly, in the ν regime where ω_E can be comparable with $< \omega_b >$, the bounce resonance presents a wider ω_E range having a significant contribution to torque than the precession resonance. In the $1/\nu$ and plateau regime, the bounce resonance induced torque decreases more quickly than the torque contributed by the precession resonance, since the bounce motion of trapped particles can be strongly affected by the collisionality. The relation between the precession resonance and the bounce resonance of trapped ions is clearly

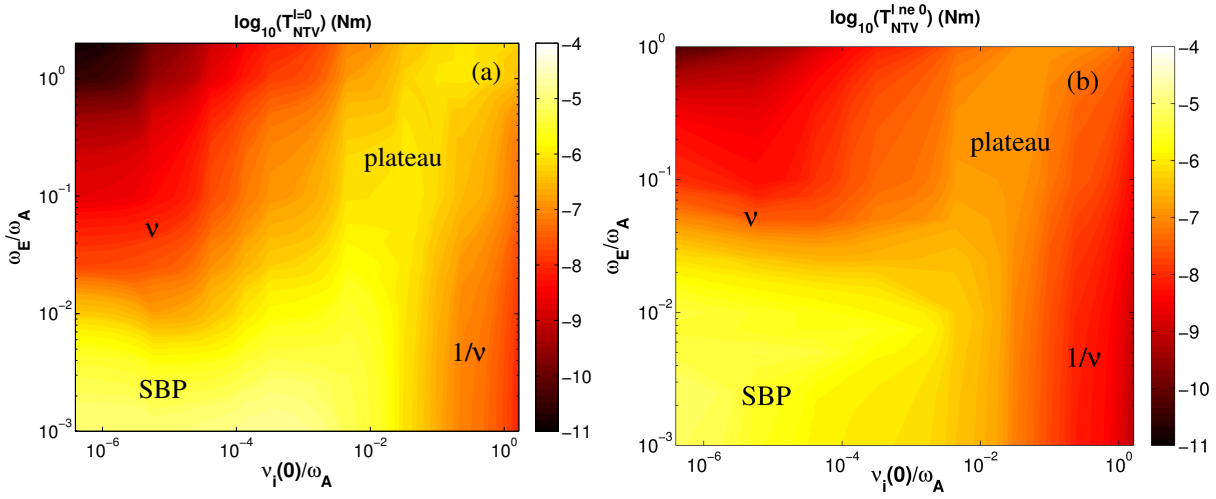

Figure 10: The ω_E and $\nu_i(0)$ dependence of NTV torque with (a) only precession resonance $T_{NTV}^{l=0}$ and (b) the bounce resonance $T_{NTV}^{l\neq 0}$. MARS-K is used to perform the computation. IPEC-PENT agrees with these results.

shown in figure 11. The ratio $T_{NTV}^{total\ l}/T_{NTV}^{l=0}$ has the maximum value in the ν region with relatively small ω_E, where $T_{NTV}^{total\ l}$ includes both precession and bounce resonances, and $T_{NTV}^{l=0}$ denotes the torque due to the precession resonance. The maximum value of $T_{NTV}^{total\ l}$ can be about 40 times larger then $T_{NTV}^{l=0}$ in the perturbed equilibrium considered here. It indicates that the bounce resonance can significantly enhance the NTV torque in the ν regime when ω_E enters the range of ion bounce frequencies with low collisionality. Similar results are also observed in experiments [4] and in particle simulations [28]. The ν regime could be important to many present tokamaks as well as ITER, particularly in the presence of sufficient momentum input.

4 Summary

In summary, we have shown the equivalence between the drift kinetic energy equation (15) used in MARS-K and the torque expression (8) in the combined NTV theory. This agrees with $T_\phi = 2in\delta W_k$ as in [3]. A successful numerical benchmarking among three different approaches of NTV theory has been carried out by applying IPEC-PENT, MARS-K and MARS-Q to the identical equilibrium. In the case of

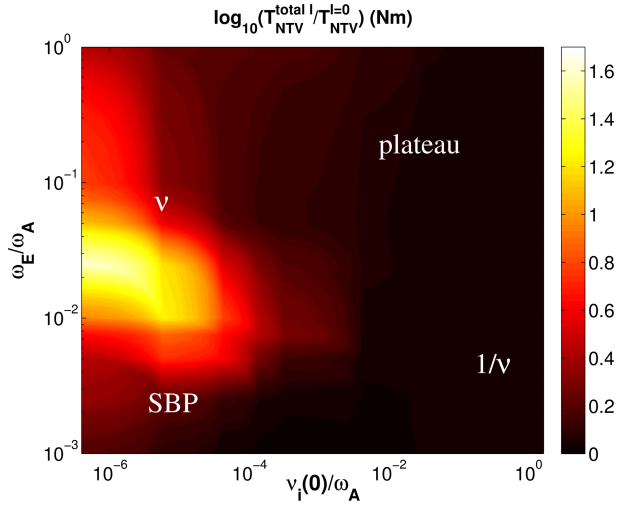

Figure 11: The ratio of torque $T_{NTV}^{total\ l}/T_{NTV}^{l=0}$ is plotted as the function of ω_E and $\nu_i(0)$. MARS-K is used to perform the computation. IPEC-PENT agrees with these results.

considering the precession resonance ($l = 0$) alone, IPEC-PENT (combined NTV) and MARS-K (equivalence between NTV torque and drift kinetic energy) show an excellent agreement as expected from our analytical derivations. The NTV torque computed by MARS-Q (connected NTV formula) also qualitatively agrees with the results of IPEC-PENT and MARS-K in different collisionality regimes. The difference is mainly due to the geometric simplification and the more complicated collisionality model used in MARS-Q. However, it is important that the tendency of torque computed by the three codes agrees well when we scan the collisionality ν_i and the $\mathbf{E} \times \mathbf{B}$ drift frequency ω_E. The NTV torque further including the bounce resonance ($l \neq 0$) is also compared between IPEC-PENT and MARS-K. Again, IPEC-PENT and MARS-K show a very good agreement. Comparing with the precession resonance case, the rotation ω_E and collisionality ν_i scan indicates that the bounce resonance can significantly enhance the NTV toruqe in the low collisionality regime ($\sim \nu$ regime) when ω_E reaches the bounce resonance condition. Although a simple equilibrium and a uniform flow have been assumed here, numerical results clearly show the importance of including the bounce resonance in NTV computation.

We point out that each of the three NTV approaches/codes considered in this

work has its own advantages and disadvantages when used for the NTV computations. In particular, IPEC-PENT and MARS-K employ full toroidal geometry, and can include both precession and bounce resonances for trapped particles. But so far only the simple Krook collisional operator has been implemented in both codes. On the other hand, the semi-analytic theory that smoothly connects various NTV regimes (as implemented in MARS-Q) includes the pitch angle scattering operator which is probably more capable of describing the particle collisions, in particular towards the lower collisionality regime (e.g. in the $\nu - \sqrt{\nu}$ regime). The semi-analytic theory has to make certain geometric simplifications. Also the present theory does not treat the particle bounce resonance. In the future, it is desirable to further advance the IPEC-PENT/MARS-K models, to include the pitch angle scattering collision. We also remark that it appears the latter may not always be important for the NTV computations. One recent example is shown in Ref. [4], where the IPEC-PENT results, with only the Krook collision but including the bounce resonances, match well with the measured NTV torque, both amplitude and profile, in KSTAR experiments.

IPEC-PENT and MARS-K both can include the kinetic effect due to passing particles, which may be important when the plasma rotation reaches above the ion acoustic speed. If the NTV torque calculation could be treated appropriately for passing particles, IPEC-PENT and MARS-K would be applied to investigate this effect. In a future study, the possibility of including the passing particle induced NTV torque will be investigated. NTV calculation is usually based on the perturbed equilibrium calculated by the fluid MHD equation (the perturbative approach). MARS-K can also include kinetic pressures $p_{\parallel}$ and $p_{\perp}$ into MHD equations self-consistently to study the MHD instability [14, 18]. Since we have demonstrated that MARS-K has the capability to perform both perturbed equilibrium and NTV torque computations, it is possible to use MAR-K to solve the perturbed equilibrium and NTV torque in a non-perturbative approach. This capability can help us to understand the interaction between the NTV torque and the plasma response particularly when β is high [29, 30]. This subject will be studied in the future work.

5 Acknowledgments

Z.R. Wang thanks Dr. Shichong Guo and Dr. John W. Berkery for very useful discussions and many helpful suggestions improving the manuscript. Y.Q. Liu would like to thank Dr. Youwen Sun for very helpful discussion on the connected NTV formula. The work was supported by DOE Contract DE-AC02-76CH03073(PPPL). This work was also part-funded by the RCUK Energy Programme under grant EP/I501045 and the European Communities under the contract of Association between EURATOM and CCFE. The views and opinions expressed herein do not necessarily reflect those of the European Commission.

References

[1] J.-K. Park, A.H. Boozer and J.E. Menard, Phys. Rev. Lett. **102**, 065002 (2009).

[2] K.C. Shaing, S.A. Sabbagh and M.S. Chu, Nucl. Fusion **50**, 025022 (2010).

[3] J.-K. Park, Phys. Plasma **18**, 110702 (2011).

[4] J. -K. Park, Y. M. Jeon, J. E. Menard, W. H. Ko, S. G. Lee, Y. S. Bae, M. Joung, K. -I. You, K. -D. Lee, N. Logan, K. Kim, J. S. Ko, S. W. Yoon, S. H. Hahn, J. H. Kim, W. C. Kim, Y. -K. Oh, and J. -G. Kwak, Phys. Rev. Lett. **111**, 095002 (2013).

[5] Y. Sun, Y. Liang, H. R. Koslowski, S. Jachmich, A. Alfier, O. Asunta, G. Corrigan, C. Giroud, M. P. Gryaznevich, D. Harting, T. Hender, E. Nardon, V. Naulin, V. Parail, T. Tala, C. Wiegmann, S. Wiesen and JET-EFDA contributors, Plasma Phys. Control. Fusion **52**, 105007 (2010).

[6] A. M. Garofalo1, K. H. Burrell, J. C. DeBoo, J. S. deGrassie, G. L. Jackson, M. Lanctot, H. Reimerdes, M. J. Schaffer, W. M. Solomon, and E. J. Strait, Phys. Rev. Lett. **101**, 195005 (2008).

[7] W. Zhu, S. A. Sabbagh, R. E. Bell, J. M. Bialek, M. G. Bell, B. P. LeBlanc, S. M. Kaye, F. M. Levinton, J. E. Menard, K. C. Shaing, A. C. Sontag, and H. Yuh, Phys. Rev. Lett. **96**, 225002 (2006).

[8] J. -K. Park, A. H. Boozer, J. E. Menard, A. M. Garofalo,M. J. Schaffer, R. J. Hawryluk, S. M. Kaye, S. P. Gerhardt, S. A. Sabbagh, and NSTXTeam, Phys. Plasmas **16**, 056115 (2009).

[9] N. C. Logan, J. -K. Park, K. Kim, Z. R. Wang, J. Berkery. "Neoclassical Toroidal Viscosity in Perturbed Equilibria with General Tokamak Geometry", Phys. Plasmas (submitted).

[10] M. S. Chu and M. Okabayashi, Plasma Phys. Controlled Fusion **52**, 123001 (2010).

[11] B. Hu and R. Betti, Phys. Rev. Lett. **93**, 105002 (2004).

[12] B. Hu, R. Betti, and J. Manickam, Phys. Plasmas **12**, 057301 (2005).

[13] Y. Q. Liu, M. S. Chu, C. G. Gimblett, and R. J. Hastie, Phys. Plasmas **15**, 092505 (2008).

[14] Z. R. Wang, S. C. Guo and Y. Q. Liu, Phys. Plasmas **19**, 072518 (2012).

[15] Z. R. Wang, S. C. Guo, Y. Q. Liu and M. S. Chu, Nucl. Fusion **52**, 063001 (2012).

[16] J. W. Berkery, S. A. Sabbagh, R. Betti, B. Hu, R. E. Bell, S. P. Gerhardt, J. Manickam, and K. Tritz, Phys. Rev. Lett. **104**, 035003 (2010).

[17] J. W. Berkery, S. A. Sabbagh, R. Betti, R. E. Bell, S. P. Gerhardt, B. P. LeBlanc, and H. Yuh, Phys. Rev. Lett. **106**, 075004 (2011).

[18] Y. Q. Liu, M. S. Chu, I. T. Chapman and T. C. Hender, Phys. Plasma **15**, 112503 (2008).

[19] Y. Q. Liu, A. Kirk and E. Nardon, Phys. Plasma **17**, 122502 (2010).

[20] F. Porcelli, R. Stankiewicz, W. Kerner, and H. L. Berk, Phys. Plasma **1**, 470(1994).

[21] K.C. Shaing, S. A. Sabbagh and M.S. Chu, Plasma Phys. Control. Fusion **51**, 035009 (2009).

[22] Y. Q. Liu, A. Kirk, and Y. Sun, Phys. Plasma **20**, 042503 (2013).

[23] Y. Q. Liu, Y. W. Sun, Phys. Plasma **20**, 022505 (2013).

[24] J.-K. Park, A. H. Boozer, and A. H. Glasser, Phys. Plasmas **14**, 052110 (2007).

[25] Y. Sun, Y. Liang, K.C. Shaing, H.R. Koslowski, C. Wiegmann, and T. Zhang, Phys. Rev. Lett. **105**, 145002 (2010).

[26] Y. Sun, Y. Liang, K.C. Shaing, H.R. Koslowski, C. Wiegmann, and T. Zhang, Nucl. Fusion **51** 053015 (2011).

[27] J. Wesson, Tokamaks (Oxford University Press, New York, 1997).

[28] K. Kim, J. -K. Park, and A. H. Boozer, Phys. Rev. Lett. **110**, 185004 (2013).

[29] A. H. Bozzer, Phys. Rev. Lett. **86**, 5059-5061 (2001).

[30] J. -K. Park, A. H. Boozer, J. E. Menard, S. P. Gerhardt, and S. A. Sabbagh, Phys. Plasmas **16**, 082512 (2009).

The Princeton Plasma Physics Laboratory is operated
by Princeton University under contract
with the U.S. Department of Energy.

Information Services
Princeton Plasma Physics Laboratory
P.O. Box 451
Princeton, NJ 08543

Phone: 609-243-2245
Fax: 609-243-2751
e-mail: pppl_info@pppl.gov
Internet Address: http://www.pppl.gov